Analyst

ROYAL SOCIETY OF CHEMISTRY

PAPER

View Article Online
View Journal | View Issue

Open Access Article. Published on 16 February 2024. Downloaded on 10/21/2025 12:17:44 AM.
This article is licensed under a Creative Commons Attribution 3.0 Unported Licence.

Check for updates

Cite this: *Analyst*, 2024, **149**, 1939

Water detection in organic solvents using a copolymer membrane immobilised with a fluorescent intramolecular charge transfer-type dye: effects of intramolecular hydrogen bonds†

Ami Morimoto,[a] Kei Shimizu,[a] Naoya Suzuki,[a] Shigeyuki Yagi,[a] Kenji Sueyoshi,[a,b] Tatsuro Endo[a] and Hideaki Hisamoto *[a]

Numerous fluorescent dye-based optical sensors have been developed to detect water in organic solvents. However, only a few such sensors can detect water in polar solvents such as methanol or dimethyl sulfoxide, and their detection range is generally narrow. Therefore, in this study, a copolymer membrane incorporated with a pyridinium betaine dye (denoted **PB1**), which exhibited intramolecular charge transfer (ICT) characteristics, was developed to realise simple water detection in organic solvents. The pyridinium betaine structure, comprising intramolecular hydrogen bonds between the oxygen in the maleimide moiety and the hydrogen in the pyridinium, was vital for achieving efficient fluorescence emission. The membrane was prepared by copolymerising **PB1** with the *N*,*N*-dimethyl acrylamide/acrylamide monomer on a glass plate, and the fluorescence in water-mixed organic solvents was investigated (λ_{abs} = 490 nm, λ_{fl} = 630 nm). The fluorescence intensity of the dye-immobilised membrane decreased with increasing water content of the organic solvents. The detection ranges in tetrahydrofuran, ethanol, methanol, and dimethyl sulfoxide were approximately <40, <40, <40, and <60 vol% water, respectively. In contrast, membranes based on a quaternary pyridinium dye (without intramolecular hydrogen bonds) did not detect water in methanol and dimethyl sulfoxide, although it was more sensitive than PB1 in the narrow region of low water concentration in THF. Theoretical calculations corroborated the importance of the pyridinium betaine structure in detecting water in organic solvents, with the increase in polarity and the formation of intermolecular hydrogen bonds between **PB1** and water found to induce molecular rotation and fluorescence quenching.

Received 14th December 2023,
Accepted 16th February 2024

DOI: 10.1039/d3an02165c

rsc.li/analyst

Introduction

Water detection in organic solvents has garnered significant interest in research and industry fields such as organic synthesis, purity measurement, and quality control. In particular, Karl Fischer (KF) titration is predominantly employed to determine the content of water in liquids, solids, and gases.[1–3] Although KF titration offers high accuracy, high precision, and a wide measurement range (water content: 1 ppm to 100%), it is somewhat inconvenient because it requires several instruments such as electrodes and involves the preparation of titration reagents. Additionally, care should be taken to ensure that interferents such as ketones, aldehydes, and redox chemicals are excluded from samples.[3–7] Although approaches to preventing the interference reaction have been explored,[8,9] simpler water detection methods are required to overcome the aforementioned difficulties.

Optical chemical sensors (optodes) have attracted considerable attention because of their simplicity;[10] therefore, numerous water-detecting optodes based on colourimetric and/or fluorescent dyes have been developed to date.[11–35] Fluorescence-based optodes are typically more sensitive than colourimetry-based optodes. The response mechanism of fluorescence-based optodes containing organic fluorophores can be classified based on the fluorescence mechanism[18,19] into photo-induced electron transfer (PET),[20–24] intramolecular charge transfer (ICT),[21,25–28] twisted ICT (TICT),[26,29,30] aggregation-induced emission (AIE),[24,29,30,32,33] and excited-state intramolecular proton transfer (ESIPT),[31,34,35] and so on. In addition to the organic-fluorophore-based water detectors, other luminescent inorganic and/or organic water detectors –

[a]*Department of Applied Chemistry, Graduate School of Engineering, Osaka Metropolitan University, 1-1 Gakuen-cho, Naka-ku, Sakai, Osaka, 599-8531 Japan. E-mail: hisamoto@omu.ac.jp*
[b]*CREST, Japan Science and Technology Agency, Japan*

† Electronic supplementary information (ESI) available. See DOI: https://doi.org/10.1039/d3an02165c

Open Access Article. Published on 16 February 2024. Downloaded on 10/21/2025 12:17:44 AM.
This article is licensed under a Creative Commons Attribution 3.0 Unported Licence.

such as graphene quantum dots,[36] carbon dots (CDs),[37–40] covalent organic frameworks (COFs),[41–44] and metal–organic frameworks (MOFs)[39,45–47] – have been developed over the past decade. Besides, applications,[18] such as inkless writing,[32,38] paper strips,[25,31–33,35,40] and luminophore-doped films[13,15,17,22,23,38] have been developed for simpler water detection as well as traditional solution-based measurement. Although various luminescent materials have been devised for water detection, most are suitable for recognising water in 1,4-dioxane, tetrahydrofuran (THF), and acetonitrile. Sensors for water detection in methanol and dimethyl sulfoxide (DMSO) have also been reported (Table 1); however, their detection range is generally narrow, the choices of fluorescence colour are limited, or the assessment typically involves solution-based measurements or paper-strip-based detection.

This study aimed at developing an optode membrane using an ICT-type dye for simple water detection in organic solvents, including polar solvents such as methanol and DMSO. ICT-type dyes are often used as chemical sensors for water detection because they are sensitive to polarity, and their absorption and/or fluorescence spectral changes depend on the solvent polarity. Additionally, they permit adjustment of the absorption and/or fluorescence bands by molecular design and exhibit low background noise owing to a large Stokes shift. However, the fluorescence intensity of ICT-type dyes occasionally diminishes in polar solvents compared to that in non-polar solvents owing to enhanced charge separation and decreased transition probability.[27,48] Therefore, ICT-type dyes are suitable for water detection in non-polar solvents but not in polar solvents. Accordingly, to achieve water detection even in polar solvents, a cyclic enolate pyridinium betaine (PB) structure was targeted in the present study (Fig. 1a). In 2021, Suzuki and Yagi *et al.* reported that PB structure has intramolecular hydrogen bonds between the carbonyl oxygen atoms of the cyclic enolate and the α-hydrogen atoms of the pyridinium ring, which suppresses TICT-induced fluorescence quenching.[49] Moreover, the same group reported that

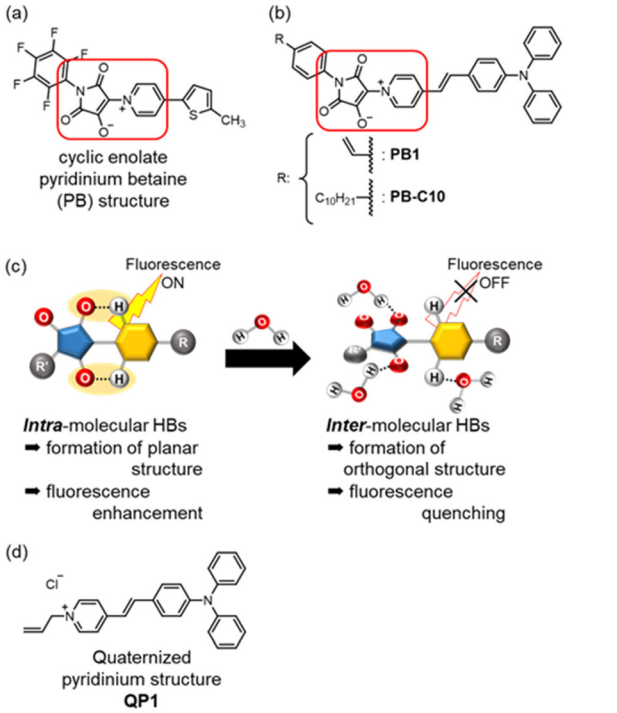

Fig. 1 (a) The pyridinium betaine (PB) structure, as reported by Suzuki and Yagi *et al.*[49] (b) The molecular design employed in the present study. (c) Concept underlying the fluorescence-based water detection (HB: Hydrogen Bond). (d) The quaternary pyridinium structure **QP1**, which was used as a reference compound.

π-extension and the introduction of a donor such as an *N*,*N*-diphenylamino group to PB structure resulted in exhibiting enhanced fluorescence; additionally, the dyes were found to exhibit solvatochromic behaviour owing to their donor–acceptor (D–A)-type structures.[50] By imparting ICT characteristics to the PB structure, the sensitivity to water and detection range would be changed. In anhydrous organic solvents, PB dyes

Table 1 Representative fluorescence-based sensors developed to detect water in methanol or DMSO

Sensing mechanism	Ref.	Solvent	Detection range	λ_{fl} (nm)	Measurement strategy other than the solution measurement scheme
AIE/PET	24	DMSO	0–1.18 wt%	510	—
ICT	25	Methanol	0–16, 60–90%	450	Paper strip detection
ICT/TICT	26	DMSO	<10 vol%	540	—
ICT/deprotonation	28	DMSO Methanol	<0.16 vol% <2.0 vol%	635–700	—
AIE	32	DMSO Methanol	—	510	Inkless writing, paper strip detection
AIE	33	DMSO	0–15 vol%	515	Paper detection
ESIPT	34	DMSO	<52 wt%	480–502	—
ESIPT	35	Methanol	0–80 vol%	454–506	Paper detection
CDs	40	Methanol	0.5–20.0 vol%	610	Paper strip detection
COF	41	Methanol	<50 vol%	380	—
MOF/ESIPT	45	Methanol	0–1.3 vol%	477	ZnO-supporting hybrid film detection
MOF/ESIPT	47	DMSO Methanol	0–5.2 vol% 0–2.2 vol%	450–540	—
ICT	Present study	DMSO Methanol	0–60 vol% 0–40 vol%	630	Copolymer membrane detection

 This journal is © The Royal Society of Chemistry 2024

Open Access Article. Published on 16 February 2024. Downloaded on 10/21/2025 12:17:44 AM.
This article is licensed under a Creative Commons Attribution 3.0 Unported Licence.

form a planar structure owing to their intramolecular hydrogen bonds, whereas in the presence of water, the intramolecular hydrogen bonds are weakened by intermolecular hydrogen bonds between the dye and water (Fig. 1c). Therefore, the PB structure would transforms into a twisted form, leading to reduced fluorescence.

In this study, a novel PB dye (**PB1**) with a terminal olefin moiety (Fig. 1b) was synthesised, and the optical and fluorescence properties in solution were measured using **PB-C10** to eliminate the influence of the terminal olefin to optical properties. Subsequently, dye-immobilised copolymer membranes were prepared[12,14] using the *N*,*N*-dimethylacrylamide (DMAA)/acrylamide (AA) comonomer to develop simple detection devices. Water detection in organic solvents was investigated using the dye-immobilised copolymer membranes. To elucidate the effects of the PB structure, a copolymer membrane immobilised quaternary pyridinium dye (**QP1**) without hydrogen bonding site was also prepared (Fig. 1d), and its sensing performance was analysed. Finally, the underlying response mechanism was clarified and then verified through theoretical calculations.

Experimental

Materials and instruments

All synthetic reagents and membrane materials were purchased from Tokyo Chemical Industry (Tokyo, Japan), FUJIFILM Wako Pure Chemical Corporation (Tokyo, Japan), or Kanto Chemical (Tokyo, Japan). All super-dehydrated organic solvents were purchased from FUJIFILM Wako Pure Chemical Corporation (Tokyo, Japan). The details of synthesis and characterization of the compounds are described in the ESI document.† UV–vis absorption spectra were acquired using a JASCO V-730 instrument, whereas fluorescence spectra were captured using a JASCO FP-8550 instrument.

Preparation of dye-immobilised copolymer membranes

Glass slide plates were cut into segments measuring 11.5 × 26.0 mm^2, which were then immersed overnight in a mixture of aqueous NaOH (1 M, 9.4 mL) and ethanol (0.6 mL). The resulting glass plates were washed with water and acetone, dried at 70 °C for 30 min, immersed in a mixture of 3-(trimethoxysilyl)propyl methacrylate (8.0 mL) and aqueous HCl (0.1 M, 2.0 mL), and then sonicated until no suspension was observed (~10 min). Finally, the methacrylated glass plates were washed with methanol and acetone and then dried at 70 °C for 30 min. Membrane mould spacers were subsequently assembled on the methacrylated glass (Fig. S1†). To that end, two layers of a 0.13 mm-thick fluoroplastic polytetrafluoroethylene film (ASF-110 FR, Chukoh Chemical Industries) with a hollowed out area measuring ~18 × 8 mm^2 were pasted onto the glass, creating a 0.26 mm-thick spacing. Approximately 40 μL of the pre-polymer solution – which comprised DMAA (0.80 mmol), AA (0.20 mmol), *N*,*N*-methylenebis(acrylamide) (5.0 μmol), azobis(isobutyronitrile) (3.0 μmol), the functional dye (0.2 μmol), water (150 μL), and 1,4-dioxane (150 μL) – was poured into the created mould, covered with an unmodified glass plates, and then polymerised at 65 °C for 45 min. The resulting membrane was washed with methanol and THF to remove unreacted reagents and then stored in super-dehydrated THF.

Preparation of sample solutions

The sample solutions – that is, mixtures of organic solvents and water with different volume ratios – were prepared immediately before the measurements to maximally prevent moisture absorption. The dye-immobilised copolymer membranes on glass plates were immersed in each sample solution for 5 min. Fluorescence spectra were acquired using a freshly prepared solution in a 10 × 10 mm^2 quartz cell, with the prepared dye-immobilised copolymer membranes on glass plates fixed diagonally across the quartz cell.

Results and discussion

Light absorption and fluorescence in solutions

To elucidate the light absorption and fluorescence properties of the functional dyes, UV–vis absorption and fluorescence spectra were acquired in chloroform ($CHCl_3$), THF, ethyl acetate (AcOEt), and DMSO (5 μM). In addition, fluorescence quantum yield (Φ_{FL}) in each solvent was investigated. The spectra and spectral data are shown in Fig. 2 and Table 2, respectively. In THF, **PB-C10** exhibited an absorption maximum (λ_{abs}) at 490 nm and a fluorescence maximum (λ_{fl}) at 600 nm; these bands can be attributed to ICT transition (*vide infra*). λ_{abs} depended minimally on the solvent polarity,

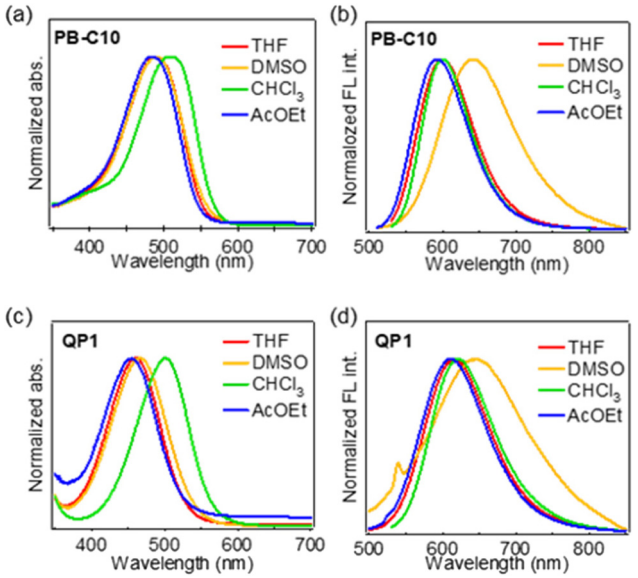

Fig. 2 (a and c) UV–vis absorption spectra and (b and d) fluorescence profiles of **PB-C10** (a and b) and **QP1** (c and d) in THF, DMSO, $CHCl_3$, and AcOEt.

Open Access Article. Published on 16 February 2024. Downloaded on 10/21/2025 12:17:44 AM.
This article is licensed under a Creative Commons Attribution 3.0 Unported Licence.

Table 2 UV–vis absorption and fluorescence properties of **PB-C10** and **QP1** in THF, DMSO, $CHCl_3$, and AcOEt

	PB-C10			**QP1**		
Solvent	λ_{abs} (nm)	λ_{fl} (nm)	Φ_{FL}	λ_{abs} (nm)	λ_{fl} (nm)	Φ_{FL}
THF	490	600	0.33	460	616	0.05
DMSO	490	641	0.04	466	647	<0.01
$CHCl_3$	510	600	0.49	500	621	0.07
AcOEt	484	593	0.26	455	612	0.05

except in the case of chloroform, whereas the λ_{fl} for DMSO was red shifted by 41 nm compared to that for THF, indicating that **PB-C10** exhibited electrically neutral ICT-type properties. Generally, the solvent polarity influences electrically neutral ICT-type dyes in the excited states to a greater extent than those in the ground states, because the former exhibit a larger dipole moment than that of the latter.[48] **QP1** tended to exhibit superior ICT properties compared with those of **PB-C10**. For instance, its λ_{abs} and λ_{fl} values in THF were blue shifted to 460 nm and red shifted to 616 nm, respectively, compared with those of **PB-C10**. The Stokes shift of **QP1** in THF (5505 cm^{-1}; 156 nm) was larger than that of **PB-C10** (3741 cm^{-1}, 110 nm). Unfortunately, the photophysical properties of **PB-C10** in more polar solvents, such as ethanol and methanol, could not be measured owing to their low solubility.

Water detection using dye-immobilised copolymer membranes

Water detection using dye solutions is inconvenient because reagent preparation must be performed on each occasion. Additionally, hydrophobic dye molecules cannot be used owing to their low solubility in water-mixed solvents, and the detection sensitivity is significantly lower than that of soluble dyes, except those with AIE luminogens. To overcome these problems, functional dyes were immobilised onto a copolymer membrane at the terminal olefin moiety on a glass plate in the present study, to enable simple detection of water in organic solvents.

First, monomer materials were selected from commercially available ones, and DMAA and AA were adopted owing to its amphiphilicity to water and organic solvents. Dye-immobilised polymer membranes with 100% DMAA or 100% AA were prepared at first in above mentioned manner. However, the former was too stiff to swell in water and peeled off from the glass plates after polymerization. The latter was successfully prepared, but peeled off from the glass plates during the experiments because volume change of the membrane by water swelling was large when water content was increased. Therefore, the two monomers, DMAA and AA, were mixed, and an appropriate molar ratio was determined to 4 : 1 which showed the most intense fluorescence (Fig. S15†) and a relatively small degree of water swelling. Similarly, the proportion of the cross-linking reagent, *N*,*N*-methylenebis(acrylamide), was also varied from 0 to 2 mol%, and the optimal addition amount was found to be 0.5 mol%. These materials were mixed with the functional dyes, and copolymer membranes were prepared following the method described in the Experimental section.

The fluorescence spectral changes of the fabricated membranes were examined in THF/water solvents (Fig. 3). Both dye-immobilised copolymer membranes (designated as **PB1**-mem and **QP1**-mem) showed decreases in the fluorescence intensity and small red shifts in λ_{fl} with increasing water content; however, the response range was different. For **PB1**-mem, as the water content increased from 0% to 100%, λ_{fl} exhibited red shifts from 591 to 627 nm, whereas the fluorescence intensity (I) decreased from 2560 a.u. (detector setting was low gain) to 11 a.u. Moreover, the fluorescence intensity of **PB1**-mem was approximately 2.6 times higher than that of **QP1**-mem (middle gain is *ca.* 10 times more sensitive than low gain). Additionally, **PB1**-mem exhibited a wide-range response (<40 vol% water), whereas **QP1**-mem showed a narrow-range response from 0 vol% (λ_{fl} = 577 nm, I = 9054 a.u.) to 10 vol% water (λ_{fl} = 613 nm, I = 324 a.u.). In other words, **QP1**-mem was more sensitive to water in THF than **PB1**-mem. To confirm the sensitivity to water, the relative fluorescence intensity with respect to the fluorescence intensity at 0 vol% water (I/I_0) was plotted against the water content (Fig. 4). At the water content of 5 vol%, the I/I_0 ratio of **PB1**-mem decreased to 0.66 at 5 vol% water content, whereas that of **QP1**-mem decreased drastically to 0.30. These results highlight the suitability of **PB1**-mem and **QP1**-mem for wide-range and low-water-content detection in THF, respectively.

The response and recovery times of **PB1**-mem were also measured. The prepared **PB1**-mem stored in THF was soaked

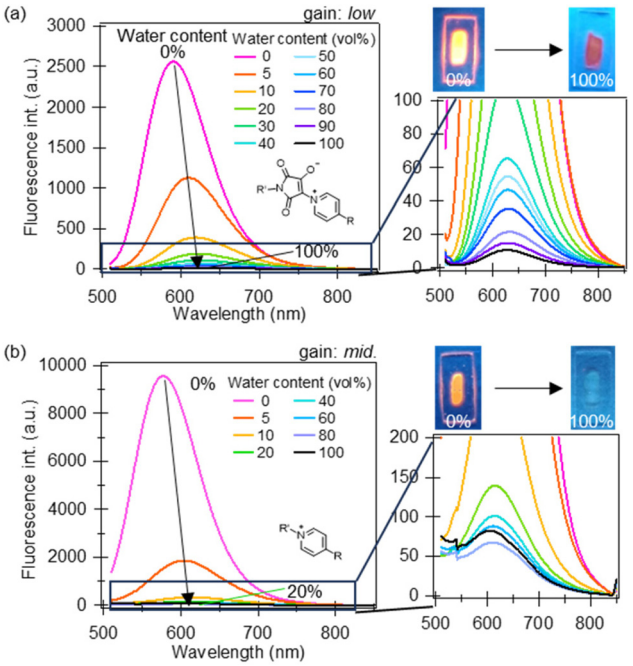

Fig. 3 Fluorescence spectra of the dye-immobilised membranes (a) **PB1**-mem (λ_{ex} = 490 nm, λ_{fl} = 630 nm) and (b) **QP1**-mem (λ_{ex} = 460 nm, λ_{fl} = 630 nm) in THF/water solvents.

Open Access Article. Published on 16 February 2024. Downloaded on 10/21/2025 12:17:44 AM.
This article is licensed under a Creative Commons Attribution 3.0 Unported Licence.

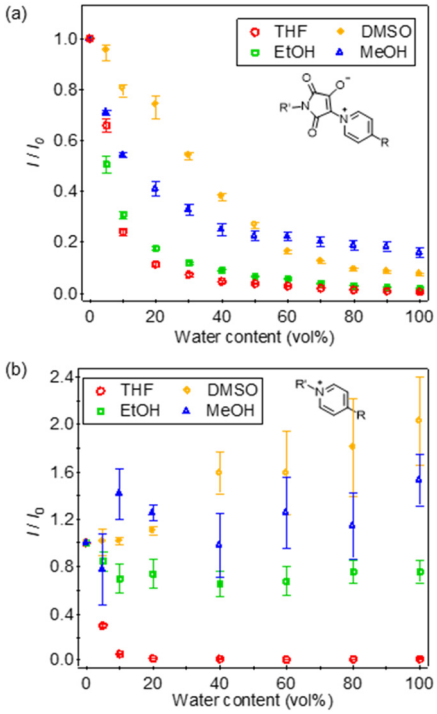

Fig. 4 Relative fluorescence intensities of the dye-immobilised membranes (a) **PB1**-mem (λ_{ex} = 490 nm, λ_{fl} = 630 nm) and (b) **QP1**-mem (λ_{ex} = 460 nm, λ_{fl} = 630 nm) in water mixed with THF, DMSO, ethanol (EtOH), and methanol (MeOH).

in a THF solution with 40 vol% water, and the fluorescence intensity at 630 nm was monitored without replacing the sample mixture (Fig. S2a†). I/I_0 reached 0.05 at 3.5 min (95% response); therefore, this value was regarded as the response time. For all other water contents, the response behaviour was almost identical, and all measurements were conducted after immersion for 5 min. The fluorescence of the membranes was recovered in a 100% THF solution, with the intensity ratio plateauing to 0.8 at 32 min without replacement of THF (Fig. S2b†). This slower recovery than response to water in anhydrous THF was presumably due to the slow spontaneous release of water molecules under static conditions. This could be improved by modifying the polymer matrix and membrane thickness and employing a flow system.

The response of the dye-immobilised membranes to water in polar solvents such as DMSO, ethanol, and methanol was examined. Membranes stored in anhydrous THF were soaked in each of the dried organic solvents for 5 min, following which the anhydrous organic solvent was replaced thrice. **PB1**-mem was excited with the excitation wavelength (λ_{ex}) of 490 nm, and its fluorescence intensity at 630 nm was monitored. Similarly, **QP1**-mem was excited at 460 nm, and the fluorescence intensity at 630 nm was investigated. **PB1**-mem achieved water detection even in methanol and DMSO (Fig. 4a), with a response range in ethanol, methanol, and DMSO of <40, <40, and <60 vol% water, respectively. In contrast, **QP1**-mem only responded to ethanol/water solvents with <10 vol% water (Fig. 4b). In the methanol/water and DMSO/water solvents, the I/I_0 value of **QP1**-mem varied owing to the considerably low fluorescence intensities. These results underscore the potency of the PB structure in enabling wide range detection of water in polar solvents, including methanol and DMSO.

The prepared membranes showed no signs of decomposition at room temperature, even without special care to oxygen, but discoloration was observed when left for several days without shading. However, when stored in anhydrous THF with shading, the same fluorescence intensity was obtained for several days, so in this study, data was acquired with the membranes stored in anhydrous THF with shading.

Effects of ICT character and PB structure on water detection in organic solvents

To gain insight into the effects of ICT character and the PB structure on its optical properties and water detection sensitivity, density functional theory (DFT) and time-dependent DFT (TD-DFT) calculations were conducted using Gaussian 09 program.[51] Optimised structures in the ground and excited states were obtained using the M06 function and 6-31G(d,p) basis sets. An alkyl group at the molecular terminal was omitted for simplification and reducing the calculation cost. Moreover, both dyes were optimised using the solvation model based on density (SMD) in THF or in water to determine the effects of solvent polarity.[52]

Optimised structures in the ground and the first excited states (S_1), as well as the distribution and the energy of the highest occupied molecular orbital (HOMO) and the lowest unoccupied molecular orbital (LUMO), were acquired for both dyes (Fig. S3 and S4†). The HOMO–LUMO transition contributed to the S_0–S_1 transition in both dyes. The predicted $\lambda_{abs,cal}$ in THF (502 and 480 nm for **PB1** and **QP1**, respectively) roughly corresponded to the experimental results (490 and 460 nm for **PB1** and **QP1**, respectively). The calculated fluorescence maxima, $\lambda_{fl,cal}$, in THF were 597 and 575 nm for **PB1** and **QP1**, respectively, and trends were different from the experimental results (600 nm and 616 nm for **PB1** and **QP1**, respectively). This would be because ICT character of **QP1** was underestimated. The HOMO of **QP1** was mainly localised at a (diphenylamino)phenyl group and the ethylene moiety, while the LUMO was distributed over a pyridinium moiety (Fig. S4†). This distribution indicated that **QP1** exhibited strong ICT characteristics, as mentioned above. The HOMO and LUMO energy levels of **QP1** were −5.45 and −2.31 eV, respectively. However, the PB structure destabilised the HOMO and LUMO, yielding values of −5.29 and −2.22 eV, respectively. The frontier orbitals of **PB1** were delocalised over the entire molecule, and the π-conjugation system extended to the maleimide moiety. To confirm the strength of ICT, the difference in dipole moment between the ground and excited states ($\mu_e - \mu_g$) was estimated from the Lippert–Mataga plot (Fig. S5†); the difference for **PB1** (20.96 D) was smaller than that for **QP1** (22.00 D). Additionally, the values of oscillator strength of **PB1** for the S_0–S_1 and S_1–S_0 transition ($f_{S_0-S_1}$ = 1.78, $f_{S_1-S_0}$ = 2.03)

Open Access Article. Published on 16 February 2024. Downloaded on 10/21/2025 12:17:44 AM.
This article is licensed under a Creative Commons Attribution 3.0 Unported Licence.

were higher than those of **QP1** ($f_{S_0-S_1}$ = 1.24, $f_{S_1-S_0}$ = 1.16). These results indicate that the ICT characteristic of **PB1** was not as prominent as that of **QP1**, and that the PB structure could be a viable candidate for achieving intense fluorescence.

Furthermore, to clarify the effects of the PB structure on the water detection sensitivity, the intramolecular hydrogen bonds between the carbonyl oxygens of the cyclic enolate and the α-hydrogens of the pyridinium ring were targeted for analysis. As reported previously,[49,50] the α-hydrogens of the pyridinium ring exhibited a large chemical shift in proton NMR to 9.73 ppm (in $CDCl_3$), whereas that of **QP1** was 9.10 ppm (in $CDCl_3$) (Fig. S14†), because the carbonyl oxygen and α-hydrogens tended to form intramolecular hydrogen bonds. The atomic distance d between the carbonyl oxygen and α-hydrogens in the theoretical optimised structure in THF (Fig. S3†) in the ground state was estimated as 2.06 Å; this value is reasonable for C–H···O interactions.[53–55] Furthermore, the increase in solvent polarity induced molecular torsion in the ground state, and d_g increased to 2.24 Å in water. The theoretical calculations also suggested that water induced molecular torsion of the PB structure, given that the dihedral angle $\varphi_{bet,g}$ between maleimide and the pyridinium ring (C–C–N–C) (Fig. S3†) increased from 1.2° in THF to −23.88° in water, and the oscillator strength decreased to 1.59. Similar trends were observed in the excited-state optimisation; d_e was increased from 2.08 Å in THF to 2.25 Å in water with the increase of $\varphi_{bet,e}$ from 6.51° in THF to −23.97° in water.

On the other hand, the SMD model could not estimate the effect of an intermolecular hydrogen bond.[52] To consider this effect, optimized structures of **PB1** with a water molecule in the ground and excited states (M06/6-31G(d,p), SMD/water) were calculated. The values of $\varphi_{bet,g}$ and $\varphi_{bet,e}$ were increased to −34.93° and −32.27°, respectively (Fig. S6†). Furthermore, the total energies in the ground state were stabilized by 4.74 kcal mol^{-1} compared to sum of the total energy of **PB1** and water (Table S1†), which energy was a reasonable value to form C–H···O interactions.[53–55] Potential energy surface scanning conducted at the M06/6-31G(d,p) level using the SMD model ($\varphi_{bet} \leq 90°$) indicated that the **PB1**–water interactions activated the molecular torsion both in the ground and the excited states (Fig. S7† and Fig. 5). In anhydrous THF, the rotational energy barrier in the excited state (ΔE_e) from the most stable state to the most unstable state ($\varphi_{bet,\ e}$ = 90°) was 6.42 kcal mol^{-1}. In the presence of a water molecule (SMD/water), ΔE_e decreased to 1.80 kcal mol^{-1}, and the distance between the oxygen in the maleimide moiety and the hydrogen in pyridinium was longer than that between the oxygen in the maleimide moiety and the hydrogen in water forming intermolecular hydrogen bonds. Similar trends were observed in the ground-state scan calculations. Unfortunately, the rupture of the intramolecular hydrogen bonds in water could not be experimentally ascertained by ^{1}H NMR spectroscopy (**PB-C10** in DMSO-d_6/water or in $CDCl_3$/methanol-d_4). Fourier-transform infrared spectroscopy of **PB1**-mem was also performed; however, no insight was acquired owing to the presence of numerous C=O bonds in the copolymer membranes. On the other hand, theoretical calculations of the vibration modes suggested the existence of interactions between the oxygen in the maleimide moiety and the hydrogen in water. The carbonyl group stretching vibrations band ($\nu_{C=O}$) for the water-free maleimide ring appeared at 1700 cm^{-1}, whereas that of the structure with water shifted to 1696 cm^{-1} (Fig. S8†). This decrease in $\nu_{C=O}$ was likely related to the intermolecular hydrogen bonds.

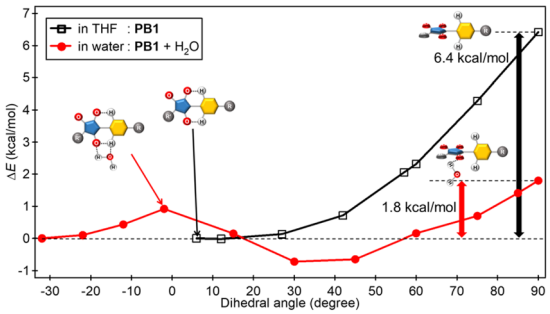

Fig. 5 Rotational energy barrier ΔE_e plotted against the dihedral angle $\varphi_{bet,e}$ between the maleimide and pyridinium rings (C–C–N–C) in the excited state.

Furthermore, effects of acid and base as impurities on fluorescence was investigated. 0.5 vol% of 1 M HCl aq. or NaOH aq. was added to anhydrous organic solvents such as THF, DMSO, *N*,*N*-dimethylformamide (DMF), and fluorescence spectra were measured. As shown in Fig. S16,† fluorescence intensities of **PB1**-mem in acid or base-added organic solvents were weaker than those in only 0.5 vol% of water-added ones. On the other hand, fluorescence intensities of **QP1**-mem in these solutions were relatively unaffected. These results would indicate that intramolecular hydrogen bonds were prevented by acid or base, and molecular torsion was promoted. Although strong and enough amount of acid or base is needed to break the intramolecular hydrogen bond at PB structure completely, but small amount is sufficient to promote molecular torsion and fluorescence decrease.

Based on experimental and computational results, the intramolecular hydrogen bonds of PB structure are important for water detection in organic solvents and permit water detection even in polar solvents such as methanol and DMSO. The addition of water, acid, and base causes the PB structure to undergo molecular torsion leading to fluorescence quenching. To further enhance the sensitivity for water detection in organic solvents, optimising the strength of the intramolecular hydrogen bonds by modifying the molecular structure and substituents could be an effective approach.

Conclusions

In this study, simple water detection in organic solvents, which have been difficult to achieve by conventional KF titration, was successfully performed using a copolymer membrane incorporated with a fluorescent pyridinium betaine dye. As the

Open Access Article. Published on 16 February 2024. Downloaded on 10/21/2025 12:17:44 AM.
This article is licensed under a Creative Commons Attribution 3.0 Unported Licence.

water content of THF/water solvent mixtures increased (0–100 vol%), the fluorescence intensity of the pyridinium betaine dye decreased and water detection was successfully realised. Notably, water detection was achieved in polar solvents such as methanol and DMSO (for <40 and <60 vol% water, respectively). On the other hand, quaternary pyridinium dye, which has only ICT character, showed more sensitive but narrow range response and was not suitable for detection of water in polar solvents compared to pyridinium betaine dye. DFT and TD-DFT calculations revealed that, in the case of pyridinium betaine dye, addition of water to organic solvents would promote molecular torsion due to the formation of intermolecular hydrogen bonds, and fluorescence decreased. To adjust sensitivity and/or response range of water detection devices, the strength of intramolecular hydrogen bonds and electron distribution should be optimised, and support materials with superior attributes should be developed.

Author contributions

A. M., K. S., T. E., and H. H. conceptualised, planned, and designed the experiments. A. M., K. S., N. S., S. Y., and H. H. conceptualised the molecular designs. A. M. performed the experiments and analysed the data. A. M., S. Y., K. S., T. E., and H. H. drafted the manuscript. All authors have approved the manuscript and agree with its submission to this journal.

Conflicts of interest

There are no conflicts to declare.

Acknowledgements

This study was partly supported by the Japan Science and Technology Agency, under the 'Establishment of University Fellowships towards the Creation of Science Technology Innovation' program (Grant No. JPMJFS2138), and the Japan Society for the Promotion of Science, through a Grant-in-Aid for Scientific Research (No. 23H01990). Authors greatly acknowledge Prof. Hiroshi Ikeda, Assoc. Prof. Yasunori Matsui, Assist. Prof. Takuya Ogaki, Assist. Prof. Kenichi Michigami, and the Analytical Centre, Graduate School of Science, Osaka Metropolitan University for kind help on characterizing synthesized molecule using mass spectrometry and elemental analysis.

References

1 K. Fischer, *Angew. Chem.*, 1935, **48**, 394–396.
2 D. M. Smith, W. M. D. Bryant and J. Mitchell, *J. Am. Chem. Soc.*, 1939, **61**, 2407–2412.
3 J. Mitchell, *Anal. Chem.*, 1951, **23**, 1069–1075.
4 F. E. Critchfield and E. T. Bishop, *Anal. Chem.*, 1961, **33**, 1034–1035.
5 E. Scholz, *Anal. Chem.*, 1985, **57**, 2965–2971.
6 A. Cedergren and C. Oraedd, *Anal. Chem.*, 1994, **66**, 2010–2016.
7 J. Hoebus, E. Roets and J. Hoogmartens, *J. Pharm. Biomed. Anal.*, 1996, **15**, 359–364.
8 K. Schmitt and H. D. Isengard, *Fresenius' J. Anal. Chem.*, 1997, **357**, 806–811.
9 F. R. van de Voort, J. Sedman, R. Cocciardi and S. Juneau, *Talanta*, 2007, **72**, 289–295.
10 P. Bühlmann, E. Pretsch and E. Bakker, *Chem. Rev.*, 1998, **98**, 1593–1688.
11 M. A. Kessler, J. G. Gailer and O. S. Wolfbeis, *Sens. Actuators, B*, 1991, **3**, 267–272.
12 H. Hisamoto, Y. Manabe, H. Yanai, H. Tohma, T. Yamada and K. Suzuki, *Anal. Chem.*, 1998, **70**, 1255–1261.
13 H. Hisamoto, H. Tohma, T. Yamada, K.-i. Yamauchi, D. Siswanta, N. Yoshioka and K. Suzuki, *Anal. Chim. Acta*, 1998, **373**, 271–289.
14 D. Citterio, K. Minamihashi, Y. Kuniyoshi, H. Hisamoto, S.-I. Sasaki and K. Suzuki, *Anal. Chem.*, 2001, **73**, 5339–5345.
15 X. Yang, C.-G. Niu, Z.-J. Shang, G.-L. Shen and R.-Q. Yu, *Sens. Actuators, B*, 2001, **75**, 43–47.
16 C. G. Niu, A. L. Guan, G. M. Zeng, Y. G. Liu and Z. W. Li, *Anal. Chim. Acta*, 2006, **577**, 264–270.
17 D. Huang, Y. Bing, H. Yi, W. Hong, C. Lai, Q. Guo and C. Niu, *Anal. Methods*, 2015, **7**, 4621–4628.
18 H. S. Jung, P. Verwilst, W. Y. Kim and J. S. Kim, *Chem. Soc. Rev.*, 2016, **45**, 1242–1256.
19 P. Kumar, A. Ghosh and D. A. Jose, *ChemistrySelect*, 2021, **6**, 820–842.
20 Y. Ooyama, A. Matsugasako, T. Nagano, K. Oka, K. Kushimoto, K. Komaguchi, I. Imae and Y. Harima, *J. Photochem. Photobiol., A*, 2011, **222**, 52–55.
21 N. Khanapurmath, M. D. Prabhu, J. Tonannavar, J. Tonannavar and M. V. Kulkarni, *J. Mol. Liq.*, 2020, **314**, 113620.
22 S. Miho, K. Imato and Y. Ooyama, *RSC Adv.*, 2022, **12**, 25687–25696.
23 N. I. Georgiev, P. V. Krasteva, V. V. Bakov and V. B. Bojinov, *Molecules*, 2022, **27**, 4229.
24 P. P. Dash, P. Mohanty, R. Behura, S. Behera, P. Singla, S. C. Sahoo, S. K. Sahoo and B. R. Jali, *J. Photochem. Photobiol., A*, 2023, **440**, 114650.
25 S. A. Yoon, J. H. Oh, S. K. Kim and M. H. Lee, *Dyes Pigm.*, 2019, **165**, 421–428.
26 T. Sachdeva and M. D. Milton, *J. Photochem. Photobiol., A*, 2020, **402.**, 112804.
27 F. Hou, X. Liu, X. Hao, G. Li, F. Lu and Q. Deng, *Dyes Pigm.*, 2021, **195**, 109667.
28 Z. Zhao, Q. Hu, W. Liu, X. Xiong, Z. Wang and H. Wang, *Dyes Pigm.*, 2023, **213**, 111186.
29 L. Cai, X. Sun, W. He, R. Hu, B. Liu and J. Shen, *Talanta*, 2020, **206**, 120214.

Open Access Article. Published on 16 February 2024. Downloaded on 10/21/2025 12:17:44 AM.
This article is licensed under a Creative Commons Attribution 3.0 Unported Licence.

30 Z. Ruan, H. Zheng, C. Deng, X. Cheng, X. Ruan, S. Lv, Y. Chen, S. Liu and J. Lin, *Dyes Pigm.*, 2022, **204**, 110476.
31 F. Wu, L. Wang, H. Tang and D. Cao, *Anal. Chem.*, 2019, **91**, 5261–5269.
32 S. K. Panda and A. K. Singh, *J. Mol. Liq.*, 2023, **375**, 121381.
33 F. Xin, J. Zhao, X. Wang, H. Wang, H. Wang, M. Xing, Y. Fu, Y. Tian and Y. Tian, *Spectrochim. Acta, Part A*, 2023, **296**, 122621.
34 J. T. Wang, Y. Y. Pei, S. F. Ren, M. Y. Yan, W. Luo, B. Zhang and Q. F. Li, *Spectrochim. Acta, Part A*, 2020, **229**, 117956.
35 G. Xiao, X. Ji, J. Ji, G. Li, G. Yang and Y. Wang, *J. Photochem. Photobiol., A*, 2023, **441**, 114714.
36 S. Tang, D. Chen, Y. Yang, C. Wang, X. Li, Y. Wang, C. Gu and Z. Cao, *J. Colloid Interface Sci.*, 2022, **617**, 182–192.
37 Q. He, S. Zhuang, Y. Yu, H. Li and Y. Liu, *Anal. Chim. Acta*, 2021, **1174**, 338743.
38 Y. Qin, Y. Bai, P. Huang and F.-Y. Wu, *ACS Appl. Nano Mater.*, 2021, **4**, 10674–10681.
39 W. Li, X. Yu, Y. Tang, Z. Li, S. J. Shah, Y. Liu, H. Zhao, M. Song, J. Li, G. Wang, L. Zhou, Z. Zhao, S. Liu and Z. Zhao, *Sens. Actuators, B*, 2023, **390**, 139954.
40 X. Mu, X. Song, D. Gao, P. Ma, Q. Wu and D. Song, *Spectrochim. Acta, Part A*, 2022, **276**, 121195.
41 Y. Chen, C. Zhang, J. Xie, H. Li, W. Dai, Q. Deng and S. Wang, *Anal. Chim. Acta*, 2020, **1109**, 114–121.
42 C. Guan, J. Cai, X. Liu and L. Guo, *Sens. Actuators, B*, 2022, **355**, 131323.
43 Z. Li, Q. Li, Z. Hu, C. Hu, X. Cui, Y. Fu and Z. Chen, *Mikrochim. Acta*, 2022, **189**, 361.
44 Z. Li, X. Cui, Z. Hu, C. Hu and Z. Chen, *Microporous Mesoporous Mater.*, 2023, **348**, 112401.
45 L. Chen, J.-W. Ye, H.-P. Wang, M. Pan, S.-Y. Yin, Z.-W. Wei, L.-Y. Zhang, K. Wu, Y.-N. Fan and C.-Y. Su, *Nat. Commun.*, 2017, **8**, 15985.
46 J. Dang, R. Zhu, W. Fang, Y. Hu, Y. Wu, S. Xin, M. Li, B. Chen, H. Zhao and Z. Li, *Dyes Pigm.*, 2022, **206**, 110602.
47 S. Y. Li, X. Yan, J. Lei, W. J. Ji, S. C. Fan, P. Zhang and Q. G. Zhai, *ACS Appl. Mater. Interfaces*, 2022, **14**, 55997–56006.
48 J. R. Lakowicz, *Principles of Fluorescence Spectroscopy*, Springer, New York, NY, 2006.
49 Y. Hayashi, N. Suzuki, T. Maeda, H. Fujiwara and S. Yagi, *New J. Chem.*, 2021, **45**, 9770–9779.
50 N. Suzuki, M. Saikusa, Y. Hayashi, T. Maeda and S. Yagi, *Dyes Pigm.*, 2023, **216**, 111291.
51 M. J. Frisch, G. W. Trucks, H. B. Schlegel, G. E. Scuseria, M. A. Robb, J. R. Cheeseman, G. Scalmani, V. Barone, B. Mennucci, G. A. Petersson, H. Nakatsuji, M. Caricato, X. Li, H. P. Hratchian, A. F. Izmaylov, J. Bloino, G. Zheng, J. L. Sonnenberg, M. Hada, M. Ehara, K. Toyota, R. Fukuda, J. Hasegawa, M. Ishida, T. Nakajima, Y. Honda, O. Kitao, H. Nakai, T. Vreven, J. A. Montgomery Jr., J. E. Peralta, F. Ogliaro, M. Bearpark, J. J. Heyd, E. Brothers, K. N. Kudin, V. N. Staroverov, R. Kobayashi, J. Normand, K. Raghavachari, A. Rendell, J. C. Burant, S. S. Iyengar, J. Tomasi, M. Cossi, N. Rega, J. M. Millam, M. Klene, J. E. Knox, J. B. Cross, V. Bakken, C. Adamo, J. Jaramillo, R. Gomperts, R. E. Stratmann, O. Yazyev, A. J. Austin, R. Cammi, C. Pomelli, J. W. Ochterski, R. L. Martin, K. Morokuma, V. G. Zakrzewski, G. A. Voth, P. Salvador, J. J. Dannenberg, S. Dapprich, A. D. Daniels, Ö. Farkas, J. B. Foresman, J. V. Ortiz, J. Cioslowski and a. D. J. Fox, *Gaussian 09, revision D.01*, Gaussian, Inc., Wallingford CT, 2009.
52 A. V. Marenich, C. J. Cramer and D. G. Truhlar, *J. Phys. Chem. B*, 2009, **113**, 6378–6396.
53 D. Ž. Veljković, G. V. Janjić and S. D. Zarić, *CrystEngComm*, 2011, **13**, 5005.
54 T. Steiner and G. R. Desiraju, *Chem. Commun.*, 1998, 891–892.
55 S. J. Grabowski, *Chem. Rev.*, 2011, **111**, 2597–2625.

 This journal is © The Royal Society of Chemistry 2024